Thermal and spectroscopic studies of 2,3,5-trisubstituted and 1,2,3,5-tetrasubstituted indoles as non-competitive antagonists of GluK1/GluK2 receptors

Bartyzel, Agata; Kaczor, Agnieszka A.; Guchowska, Halina; Pitucha, Monika; Wróbel, Tomasz M.; Matosiuk, Dariusz

CrossMark

Thermal and spectroscopic studies of 2,3,5-trisubstituted and 1,2,3,5-tetrasubstituted indoles as non-competitive antagonists of GluK1/GluK2 receptors

Agata Bartyzel[1] · Agnieszka A. Kaczor[2,3] · Halina Głuchowska[1] · Monika Pitucha[4] · Tomasz M. Wróbel[2,5] · Dariusz Matosiuk[2]

Abstract

This paper reports the thermal stability and thermal degradation of six derivatives of indole by means of TG-DSC (in air) and TG-FTIR (in nitrogen) techniques. The compounds were also characterized by infrared spectroscopy. In addition, IR spectra were calculated and compared with the experimental data. In particular, the potential energy distribution analysis was performed to assign IR signals. The studied compounds are characterized by good thermal stability in oxidizing and inert atmospheres which is important for potential medical application. Thermogravimetric measurements in air atmosphere showed that the decomposition of compounds proceeds in two or three main stages. The thermal degradation of compounds is preceded by the melting process. The pyrolysis of samples is a one-step process. Together with the analyses performed in nitrogen, the FTIR spectra of the evolved gas phase products were recorded. On the FTIR spectra of gaseous products, only the bands of water, carbon dioxide and carbon oxide molecules are present. In the case of indole derivatives containing the *p*-chlorobenzyl substituent in position 1, the bands of anisole, *p*-chlorotoluene and chlorobenzene also appear.

Keywords Indole derivatives · Thermal behaviour · IR spectra · PED analysis · Theoretical computations · Non-competitive antagonists of GluK1/GluK2 receptors

Introduction

Indole is a well-known and important privileged structure scaffold found in many natural and synthetic compounds. This core is recognized as one of the foremost biologically significant moieties in nature. The indoles are characterized by excellent binding affinity for various receptors [1, 2]. The indole-based compounds can also exhibit various biological activities such as anti-inflammatory, analgesic, antifungal, antimicrobial, insecticidal, antioxidant, antiviral, antidepressant, antiarrhythmic, antihistaminic and antidiabetic ones. [3–6]. According to the literature, there are over ten thousand biologically active compounds containing indole core. More than 200 of them were approved as commercially available drugs or are undergoing clinical

✉ Agata Bartyzel
agata.bartyzel@poczta.umcs.lublin.pl

1 Department of General and Coordination Chemistry, Maria Curie-Skłodowska University, Maria Curie-Sklodowska Sq. 2, 20031 Lublin, Poland

2 Department of Synthesis and Chemical Technology of Pharmaceutical Substances with Computer Modeling Laboratory, Faculty of Pharmacy with Division of Medical Analytics, Medical University, 4a Chodzki St., 20093 Lublin, Poland

3 Department of Pharmaceutical Chemistry, School of Pharmacy, University of Eastern Finland, Yliopistonranta 1, P.O. Box 1627, FI-70211 Kuopio, Finland

4 Department of Organic Chemistry, Faculty of Pharmacy with Division of Medical Analytics, Medical University, 4a Chodzki St., 20093 Lublin, Poland

5 Department of Drug Design and Pharmacology, Faculty of Health and Medical Sciences, University of Copenhagen, Universitetsparken 2, 2100 Copenhagen Ø, Denmark

trials [7, 8], e.g., vinblastine (anticancer), indomethacin (anti-inflammatory), arbidol (antiviral), delavirdine (anti-HIV), zafirlukast (anti-asthmatic), pravadoline (analgesic), bucindolol (β-blocker) and roxindole (schizophrenia) [4–6]. The indoles are also used as dyes, pigments, plastics, fungicides, vitamin supplements, flavour enhancers, and perfumery [9].
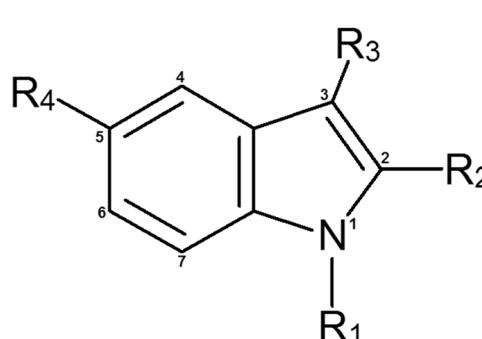
The main aim of this research was the thermal and spectroscopic characterization of six indole derivatives, i.e., 5-methoxy-2-(4-methoxyphenyl)-3-methylindole (**1**), 1-ethyl-5-methoxy-2-(4-methoxyphenyl)-3-methylindole (**2**), 1-[(4-chlorophenyl)methyl]-5-methoxy-2-(4-methoxyphenyl)-3-methylindole (**3**), 1-ethyl-2-(4-methoxyphenyl)-3-methylindole (**4**), 1-ethyl-2-phenyl-5-methoxy-3-methylindole (**5**) and 11-ethyl-8-methoxy-6,11-dihydro-5*H*-benzo[*a*]carbazole (**6**) (Scheme 1). The investigated compounds were synthesized in the Fisher indolization reaction from the respective arylhydrazine hydrochloride and appropriate ketone in anhydrous boiling ethanol saturated with HCl followed by alkylation with alkyl halide (with application of sodium hydride). These compounds are a non-competitive antagonists of kainate GluK1/GluK2 (GluK—glutamatergic kainate receptors) receptors with low micromolar activity, and compound **2** is the most promising from the series [10, 11]. Non-competitive antagonists of kainate receptors [10–15] can be considered promising compounds for the treatment of neurodegenerative diseases [16, 17] as well as epilepsy [18]. In particular, a non-competitive mode of action can result in a better safety profile as reported for non-competitive antagonists of α-amino-3-hydroxy-5-methyl-4-isoxazolepropionic acid (AMPA) receptors [19]. In the previous studies, we also constructed 3D models of GluK1 and GluK2 receptors and suggested that indole-derived non-competitive antagonists can bind in the receptor transduction domain [11, 14, 15, 20, 21]. In this study, in
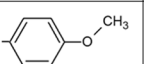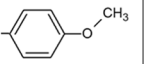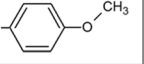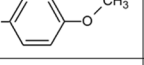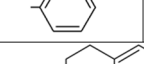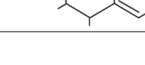
order to investigate thermal behaviour of indole derivatives the TG-DSC and TG-FTIR methods were applied. The compounds were also characterized by infrared spectroscopy. In addition, infrared (IR) spectra of the studied indole derivatives were calculated and compared with the experimental data. Theoretical vibrational spectra of the compounds were interpreted in terms of potential energy distribution (PED) analysis. Shortly, in order to describe the vibration of a *N*-atomic molecule using the PED analysis, the construction of the set of 3N-6 local, linearly independent, internal coordinates is required [22]. This set represents stretching, bending and deformation motions of the functional groups or the chosen fragments of the molecule [22]. The availability of such a coordination set instead of the normal modes causes that the potential energy distribution matrix, the PED matrix, ceases to be diagonal, but the energy distribution originating from the motions of particular functional groups is understandable for the interpreter [22]. The rationale of the performed research results from the necessity of thermal stability of the compounds under investigations which is important for their potential biomedical application.

Experimental

Synthesis and short description of compounds 1–6

The investigated compounds were synthesized according to the following procedure: the mixture of 0.05 mol of arylhydrazine hydrochloride, 0.05 mol of ketone, 100 cm^3 of anhydrous ethanol and 10 cm^3 of ethanol saturated with HCl was refluxed for 4 h. The reaction mixture was left overnight at room temperature. The obtained product was

Compound	R$_1$	R$_2$	R$_3$	R$_4$
1	–H	(4-methoxyphenyl, –O–CH$_3$)	–CH$_3$	–OCH$_3$
2	–C$_2$H$_5$	(4-methoxyphenyl, –O–CH$_3$)	–CH$_3$	–OCH$_3$
3	–CH$_2$–(phenyl)–Cl	(4-methoxyphenyl, –O–CH$_3$)	–CH$_3$	–OCH$_3$
4	–C$_2$H$_5$	(4-methoxyphenyl, –O–CH$_3$)	–CH$_3$	–H
5	–C$_2$H$_5$	(phenyl)	–CH$_3$	–OCH$_3$
6	–C$_2$H$_5$	(fused tetrahydronaphthalene)		–OCH$_3$

Scheme 1 The studied indoles
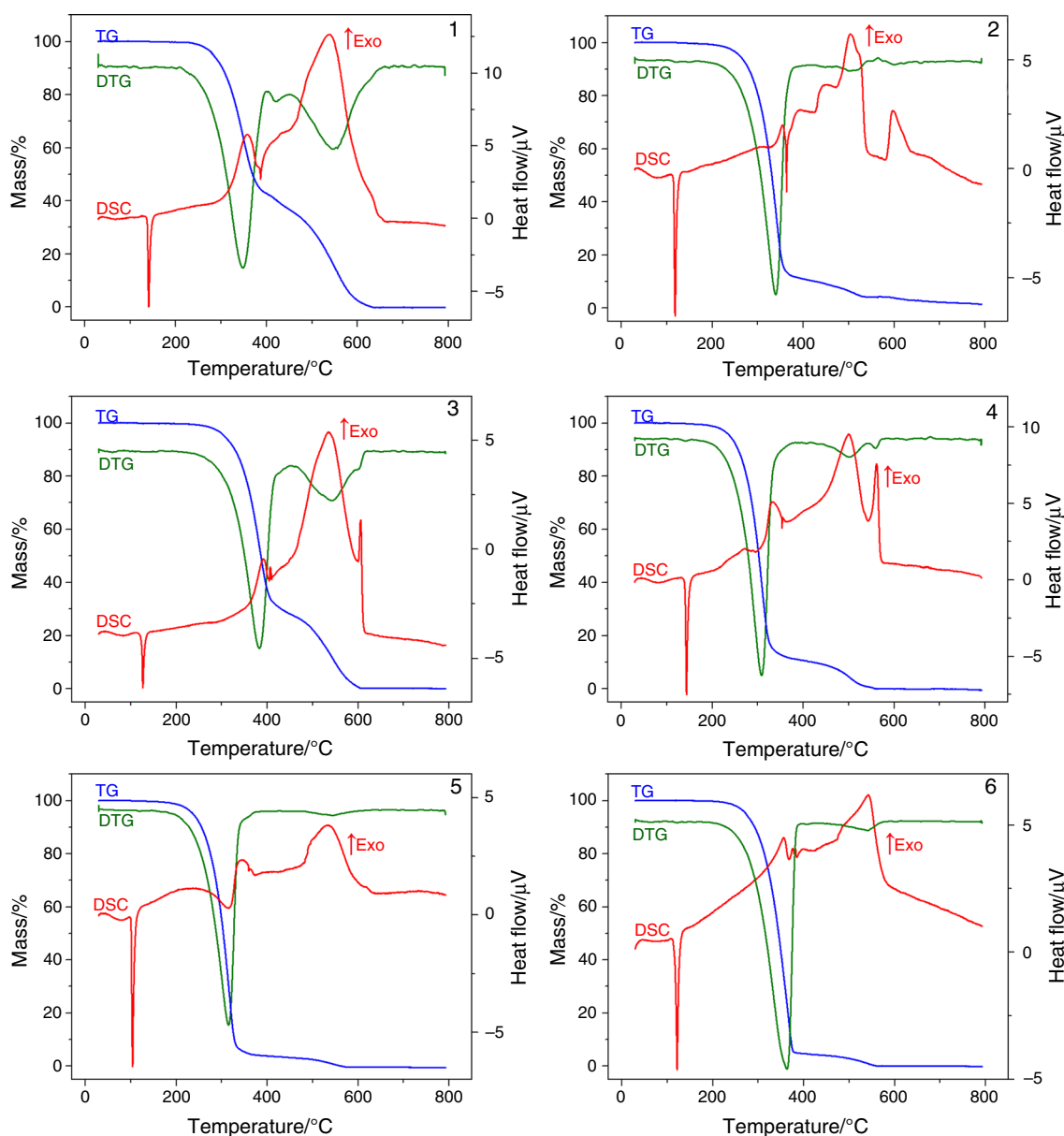
Fig. 1 TG, DTG and DSC curves recorded for **1–6** in air atmosphere

Table 1 Results of the melting process

Sample	T_{onset}/°C	T_{peak}/°C	ΔH_m/J g^{-1}	ΔH_m/J mol^{-1}
1	137	141	82.21	21.98
2	115	118	71.92	21.23
3	124	127	48.94	19.14
4	140	143	82.64	21.91
5	100	104	71.02	18.83
6	117	122	69.51	19.26

filtered and purified by crystallization from ethanol and washed with *n*-hexane. In the next step, 0.01 mol of the indole derivative was dissolved in 30 cm^3 of anhydrous *N*,*N*-dimethylformamide (DMF). The reaction mixture was cooled to 0 °C, and 0.8 g of sodium hydride was added (50% oil suspension). After 30 min of mixing, a solution of 0.012 mol of alkyl halide in 20 cm^3 of anhydrous DMF was added dropwise. The reaction was allowed to continue at room temperature for 3 h. The mixture was filtered, and 30–40 cm^3 of water was added to the filtrate. The obtained precipitate was filtered off and purified by crystallization from ethanol and washed with *n*-hexane. The detailed physicochemical and spectral properties of the investigated compounds were described in the previous paper [10].

Table 2 Thermal analysis data for compounds **1–6**

| Complex	Atm	Temperature range/°C	T_{peak}/°C	Mass loss/%
1	Air	222–398	348	56.98
		398–652	421; 548	43.02
	N_2	207–410	350; 373	98.51
2	Air	205–398	339	89.97
		398–537	503; 515	5.81
		587–787	600	2.73
	N_2	193–360	331; 346	98.46
3	Air	251–435	383	70.40
		435–612	542; 598	29.58
	N_2	234–444	379	99.00
4	Air	182–381	309	88.73
		381–540	503	10.40
		540–570	559	0.84
	N_2	167–334	256; 344	99.52
5	Air	182–384	315	95.93
		484–603	544	4.07
	N_2	164–310	299	99.94
6	Air	217–390	363	95.09
		463–575	543	4.90
	N_2	200–370	360	99.93

Atm atmosphere of analysis, T_{peak} DTG peak temperature (maximum change of mass)

Methods and physical measurements

The thermal behaviour of compounds was studied in air and nitrogen atmospheres. The thermal stability and decomposition in oxidizing atmosphere were determined using the Setaram Setsys 16/18 derivatograph. The TG and DSC curves were recorded in temperature range between 30 and 800 °C. The samples (6.18–7.56 mg) were heated in a ceramic crucible at the heating rate of 10 °C min^{-1} in flowing air (v = 0.75 dm^3 h^{-1}). The temperature and heat flow of the instrument were calibrated by the melting point
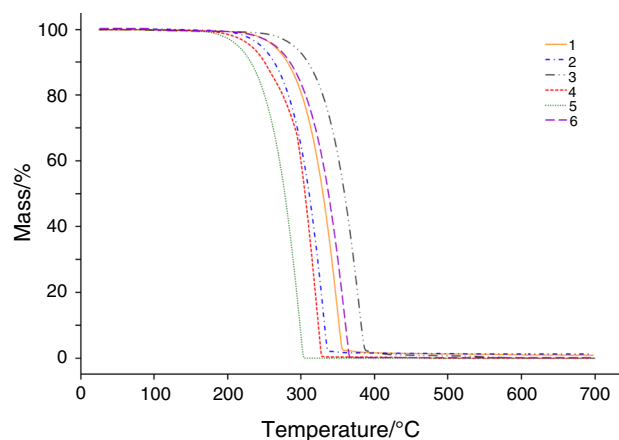
Fig. 2 TG curves of **1–6** in nitrogen

and enthalpy of indium standard. The studies in inert atmosphere were carried out using the TGA Q5000 analyser (TA Instruments, New Castle, Delaware, USA). The compounds (15.14–29.69 mg) were heated in an open platinum crucible from ambient temperature ($\sim$ 23–25 °C) to 700 °C in flowing nitrogen (25 cm^3 min^{-1}). Simultaneously with the TG analysis in nitrogen, the infrared spectra of gaseous products were recorded using the Nicolet 6700 FTIR spectrophotometer (Thermo Scientific) in the spectral range of 600–4000 cm^{-1} with a resolution of 4 cm^{-1} and 6 scans per spectrum. ATR-FTIR spectra were collected using the Thermo Scientific Nicolet 6700 FTIR spectrometer equipped with a Smart iTR diamond ATR accessory in the range from 4000 to 500 cm^{-1}. The samples were placed directly on the diamond crystal of ATR accessory, and the spectra were obtained from 16 scans taken at a resolution of 4 cm^{-1} and normalized.

Computational studies

Energy and geometry of compounds **1–6** were optimized with the B3LYP DFT method (DFT—density functional
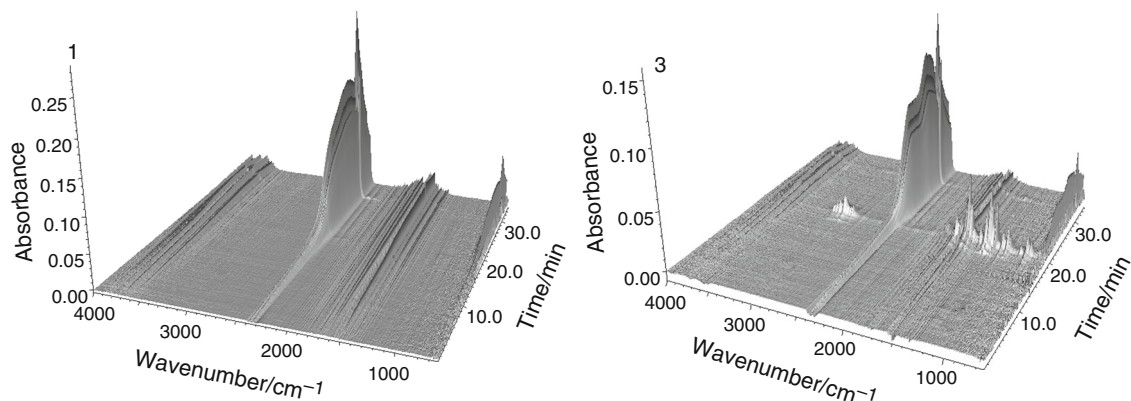
Fig. 3 3D FTIR spectra of pyrolysis products during the thermal degradation of **1** and **3**
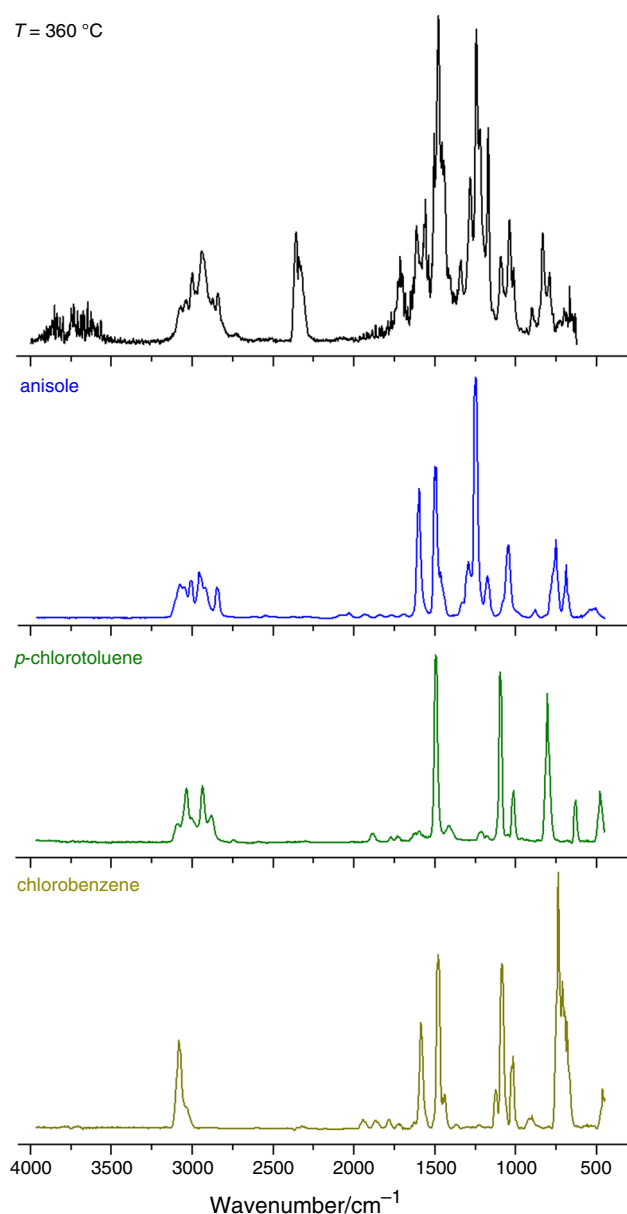
T = 360 °C

anisole

p-chlorotoluene

chlorobenzene

Fig. 4 FTIR spectrum of volatile products of thermal decomposition of **3** recorded at 360 °C and the spectra of anisole, p-chlorotoluene and chlorobenzene

theory) and the 6-311G++(2df, 2pd) basis set of Gaussian09 software [23]. Gaussian09 was also used to calculate IR spectra. The computed IR spectra were corrected using the scaling factor of 0.962 as recommended for this level of theory [24]. Moreover, the computed vibrational frequencies have been unambiguously assigned by means of the potential energy distribution (PED) analysis of all the fundamental vibration modes by using VEDA 4 program [25, 26] as described previously [27–30].

Results and discussion

Thermal behaviour of 1–6

The TG-DSC curves providing information about the thermal properties of **1–6** are shown in Fig. 1. As it can be seen in the TG curves, the compounds are characterized by good thermal stability, which is a very important parameter for their potential application as drugs. The first changes are recorded on the DSC curves as endothermic peaks at temperature 100–140 °C. These peaks are not accompanied by a mass loss and can be attributed to the melting process. They are roughly similar to the values reported earlier and determined using a Boetius apparatus [10]. The melting point onset temperature (T_{onset}), peak temperature (T_{peak}) corresponding to each peak, and enthalpy of fusion taken from the DSC curves for all compounds are listed in Table 1. The melting peaks are sharp which indicates that the compounds were probably synthesised as pure, crystalline substances [31–33]. Generally, the substitution of the pyrrole hydrogen atom in position 1 leads to a decreased melting point. The exception is compound **4** where the melting point is comparable to that of compound **1**. This can be a result of a lack of a substituent in the 5-position of the indole core.

The decompositions of the compounds in air are two- or three-step processes that are noted on the TG curves (see Fig. 1). For all compounds, the major mass loss (56.98–95.93%) occurs in the first stage which starts at 183–251 °C (Table 2). Taking into account the initial temperature of the decomposition processes, the following relative thermal stability order: **5 = 4 < 2 < 6 < 1 < 3** can be established. As can be observed, the substitution of hydrogen attached to nitrogen atom with the ethyl group decreases the combustion temperature of compounds while the p-chlorobenzyl substituent stabilizes the molecule and increases the decomposition temperature of **3** in air compared to **1**. In the case of compounds **1** and **3**, probably during the first stage the substituents of the indole core are broken off and combusted. The theoretical values of the indole residue (C_8H_7N) are 43.82 and 29.95% while the experimental ones are equal to 43.03 and 29.60% for compounds **1** and **3**, respectively. The formed products are unstable and immediately undergo complete destruction and combustion accompanied by a significant exothermic effect. The samples are fully decomposed at 612–652 °C. It is worth mentioning that for compound **1** on the DTG curve two maxima are visible during this stage, but this is not clearly indicated on the TG curve. The remaining compounds are almost completely decomposed during this step (more than 85% of overall mass is lost), and the formed residues are combusted during one (**5** and **6**) or two (**2** and

Table 3 Experimental and computed IR frequencies and PED assignment of signals for compound **2** (the most promising compound within the studied series)

Experimental	Computed		
	Raw	Scaled	PED
	3241	3117	νCH (99)
	3215	3092	νCH (94)
	3211	3089	νCH (92)
	3197	3075	νCH (99)
	3189	3068	νCH (99)
	3182	3061	νCH (92)
	3180	3059	νCH (94)
	3177	3056	νCH (99)
	3135	3015	νCH (92)
	3124	3005	νCH (99)
2996 (m)	3123	3004	νCH (92)
	3103	2985	νCH (99)
	3100	2982	νCH (83)
2951 (m)	3066	2949	νCH (100)
	3055	2939	νCH (88)
2830 (w)	3051	2935	νCH (99)
1898 (vw)	3037	2922	νCH (99)
1868 (vw)	3009	2895	νCH (92)
1835 (vw)	2999	2885	νCH (93)
1612 (m)	1658	1595	νCC (60)
1588 (w)	1650	1587	νCC (31)
1576 (w)	1610	1549	νCC (19)
1562 (w)	1604	1543	νCC (35)
1506 (m)	1580	1520	νCC (45)
1481 (s)	1538	1480	δHCC (12)
	1513	1456	δHCH (53)
	1510	1454	δHCH (45)
1448 (s)	1507	1448	δHCH (61), ΓHCOC (10)
	1502	1445	δHCH (12)
	1497	1440	δHCH (70)
	1496	1439	δHCH (75), ΓHCOC (16)
	1495	1438	δHCH (78), ΓHCOC (14)
1431 (m)	1493	1436	δHCH (72), ΓHCCN (15)
	1481	1425	νCC (33), δHCC (10)
	1479	1423	δHCC (76)
1418 (m)	1473	1417	δHCC (10), δHCH (48)
1386 (m)	1446	1391	νCC (32), δHCC (22)
1377 (w)	1421	1367	δHCC (17)
1366 (m)	1412	1358	δHCH (82)
1351 (m)	1400	1347	δHCH (15), ΓHCNC (30)
	1374	1322	νNC (26)
1307 (m)	1356	1304	νCC (33), δHCC (12)
1286 (s)	1337	1286	δHCC (72)
	1325	1275	δCCC (10)
	1318	1268	νCC (17), δCCC (11)
1246 (s)	1303	1253	δHCC (22), ΓHCNC (10)
1231 (vs)	1276	1228	νCC (28), νOC (32)
	1261	1213	νCC (11), δHCC (10)

Table 3 continued

Experimental	Computed		
	Raw	Scaled	PED
1202 (s)	1251	1203	νOC (20), δHCC (28)
1182 (m)	1213	1167	νOC (26)
1171 (s)	1205	1159	δHCH (17), ΓHCOC (58)
	1201	1155	δHCH (10),), ΓHCOC (32)
1142 (m)	1198	1153	δHCC (51)
	1174	1130	νCC (15), δHCC (36)
	1173	1128	δHCH (29), ΓHCOC (67)
1108 (m)	1166	1122	δHCC (26)
	1134	1091	δHCC (25)
1072 (s)	1096	1054	νCC (19), ΓHCCN (39)
1035 (vs)	1067	1027	νOC (64)
	1064	1024	νOC (53), δHCC (13)
1003 (w)	1025	986	δCCC (43)
963 (vw)	993	955	ΓHCCC (70), ΓCCCC (13)
948 (w)	969	932	ΓHCCC (71)
	955	919	νCC (44), δCCC (15)
	950	914	νCC (45), δCCN (12)
895 (m)	927	892	ΓHCCC (85), ΓCCCC (11)
848 (m)	887	853	ΓHCCC (71)
833 (s)	868	835	ΓHCCC (65)
818 (s)	862	829	ΓHCCC (54), ΓOCCC (17)
794 (vs)	832	800	ΓHCCC (100)
	810	779	ΓHCCC (48)
775 (m)	807	776	νCC (24), νOC (14), ΓHCCC (11)
	797	766	ΓHCCC (84)
	785	755	νNC (11), ΓHCCN (10)
	780	750	νCC (13), δCCC (12)
738 (w)	761	732	ΓCCCC (69)
702 (m)	752	723	ΓCCCC (34)
	699	672	ΓCNCC (34)
658 (w)	675	649	νNC (11), ΓCNCC (12)
630 (m)	654	629	δCCC (11)
617 (w)	642	617	δCCC (31), ΓCNCC (10)
606 (m)	632	608	ΓHCCC (14), ΓCCCC (34), ΓOCCC (20)
583 (w)	597	574	δCCC (12), δOCC (11)
564 (w)	575	553	ΓOCCC (10)
526 (vw)	551	530	δCCC (14), δCOC (21)
	519	499	ΓOCCC (20)
	488	469	δOCC (21), δCOC (18)
	470	452	δCCN (21)
	447	430	ΓHCCC (11), ΓCCNC (14), ΓCCCC (36), ΓOCCC (13)
	433	417	ΓHCCC (32), ΓCCCC (58)
	404	389	δCOC (10)
	366	352	δCCN (23), ΓCNCC (10)
	359	345	δCOC (10), ΓOCCC (11), ΓCCCC (10)
	337	324	δCCC (12), ΓCCCN (15), ΓOCCC (16)
	311	299	δCNC (26), ΓHCCN (10)
	265	255	δOCC (20), δCOC (13), ΓCCNC (10)

Table 3 continued

Experimental	Computed		
	Raw	Scaled	PED
	250	241	ΓHCOC (64)
	228	219	δOCC (14), ΓHCOC (10), ΓHCCN (13)
	213	205	vCC (19), δCCC (11)
	195	188	δCNC (19), ΓHCCN (11)
	190	183	δOCC (13), ΓCCNC (14)
	147	141	δCCC (10), ΓCOCC (10)
	95	91	ΓCOCC (55)
	81	78	ΓCOCC (25), ΓCCCN (35)
	67	64	ΓCOCC (27), ΓCCNC (11), ΓCCCN (22)
	60	58	ΓNCCC (44), ΓCCCC (10)
	55	53	ΓCOCC (13), ΓCCNC (39)
	37	36	δNCC (14), δCCC (16), ΓCNCC (18), ΓNCCC (22)
	32	31	ΓCNCC (18), ΓNCCC (13), ΓCCCC (23)

s Strong, *m* medium, *w* weak, *v* very, *br* broad, *sh* shoulder, *v* stretching, *δ* bending in plane, *Γ* torsional vibrations

4) steps. Compounds **4**, **5** and **6** are fully combusted at a temperature of 570–603 °C. In the case of **2**, it was found that under the measuring conditions a small amount of unburnt organic matrix remains (1.49%).

Thermal behaviour of **1–6** was also studied in nitrogen atmosphere (see Fig. 2). The order of thermal stabilities in inert and oxidizing atmospheres is similar; taking into account the initial temperature of the decomposition processes under nitrogen stream, the following relative thermal stability order: **5 ≈ 4 < 2 < 6 < 1 < 3** can be established. In contrast to the thermal decomposition in air, the pyrolysis processes start at a lower temperature (about 12–22 °C) than the combustion ones. Thermal decompositions of compounds in nitrogen proceed in one major mass loss step and similar to the combustion, the compounds are almost completely burnt (for compound **2** the residue after the pyrolysis is 1.54%). The total pyrolysis of the compounds can be associated with the presence of methoxy groups as observed for other compounds containing such substituent [30, 31]. Simultaneously with the TG analysis in nitrogen, the FTIR spectra of gaseous products were recorded. The FTIR spectra of gaseous products evolved during the decomposition of compounds **1** and **3** are given in Fig. 3. In the spectra of gaseous products, except for the compound **3**, only the bands characteristic of water, carbon monoxide and carbon dioxide were present. The peaks at 2240–2400 cm^{-1} are assigned to stretching vibration v(C–O) of carbon dioxide molecule. In addition, a band at 669 cm^{-1} is observed due to the deformation vibration of CO_2. The double peaks in the range 2050–2275 cm^{-1} correspond to the vibrations of CO molecule. The characteristic bands of water molecules are observed in the range 3450–4000 and 1300–1950 cm^{-1}

for stretching and deformation vibrations, respectively [31, 32, 34]. Probably other compounds such as indole can be condensed in the transfer line and do not reach the detector. In the case of compound **3**, at a temperature between 340 and 420 °C of the pyrolysis process on the FTIR spectra of evolved gases, several bands in the range 2700–3100 and 750–1800 cm^{-1} were recorded. These peaks are probably due to the presence of anisole, *p*-chlorotoluene and chlorobenzene (see Fig. 4).

Infrared spectroscopy

The FTIR spectra of **1–6** are given in Figs. S1–S6. The observed and calculated frequencies in the infrared spectra of studied compounds together with their PED assignment of signals are presented in Tables 3 and S1–S5 (Supplementary material). The scaled computed IR spectra are in accordance with the experimental values. The strong, sharp peak at 3379 cm^{-1} in the FTIR spectrum of **1** is characteristic of v(N–H) vibrations of the pyrrole ring. This is consistent with the literature data; the indoles unsubstituted in the l-position (N) give a sharp absorption peak in the range 3500–3300 cm^{-1} [35–40]. This band was not recorded in the spectra of other studied compounds due to the substitution of hydrogen atom in position 1 by ethyl or 4-chlorobenzyl group. The peaks at 3100–2990 cm^{-1} can be assigned to the C–H stretching vibrations of the aromatic bonds. The symmetric and asymmetric C–H stretching bands of the methyl/ethyl groups are observed in 2990–2800 cm^{-1}. The other important peaks are observed at the range 1620–1400 cm^{-1}, and they are mainly due to the stretching vibrations v(CC) of indole and benzene rings. The varying intensity bands observed in the FTIR spectra

at 1373–1342 and 1287–1283 cm^{-1} can be assigned to the C–N stretching modes of pyrrolic ring. These assignments are in agreement with the literature [35, 39, 41] and correlate with the theoretical calculations. The remaining bands characteristic of **1–6** with their detailed description is given in Tables 3 and S1–S5.

Conclusions

Thermal analysis of six indoles derivatives was performed. The investigated compounds are stable at room temperature which is important for their medical application. The DSC melting peaks of compounds are sharp indicating that they are probably crystalline, pure substances. In air atmosphere, the decomposition process of **1–6** occurs in two or three stages where the main mass loss occurs during the first one. On the basis of the TG-DSC analysis, it can be concluded that the substitution of hydrogen atom by the ethyl group on the pyrrole ring in 1 position leads to decrease in the thermal stability of the studied indoles. Changing the substituent to the *p*-chlorobenzyl group causes the compound stabilization and, consequently, an increase in the decomposition temperature of **3** compared to that of the other compounds. The performed TG-FTIR analysis showed there are no residual solvents in the structure of studied compounds.

References

1. Dalpozzo R, Bartoli G, Bencivenni G. Recent advances in organocatalytic methods for the synthesis of disubstituted 2- and 3-indolinones. Chem Soc Rev. 2012;41:7247–90.
2. Evans BE, Rittle KE, Bock MG, Dipardo RM, Freidinger RM, Whitter WL, Lundell GF, Veber DF, Anderson PS, Chang RSL, Lotti VJ, Cerino DJ, Chen TB, Kling PJ, Kunkel KA, Springer JP, Hirshfield J. Methods for drug discovery: development of potent, selective, orally effective cholecystokinin antagonists. J Med Chem. 1988;31:2235–46.
3. Sharma V, Kumar P, Pathak D. Biological importance of the indole nucleus in recent years: a comprehensive review. J Heterocycl Chem. 2010;47:491–502.
4. Kaushik NK, Kaushik N, Attri P, Kumar N, Kim CH, Verma AK, Choi EH. Biomedical importance of indoles. Molecules. 2013;18:6620–62.
5. Chadha N, Silakari O. Indoles as therapeutics of interest in medicinal chemistry: bird's eye view. Eur J Med Chem. 2017;134:159–84.
6. Biswal S, Sahoo U, Sethy S, Kumar HKS, Banerjee M. Indole: the molecule of diverse biological activities. Asian J Pharm Clin Res. 2012;5:1–6.
7. Bartoli G, Dalpozzo R, Nardi M. Applications of Bartoli indole synthesis. Chem Soc Rev. 2014;43:4728–50.
8. Dalpozzo R. Strategies for the asymmetric functionalization of indoles: an update. Chem Soc Rev. 2015;44:742–78.
9. Barden TC. Indoles: industrial, agricultural and over-the-counter uses. Top Heterocycl Chem. 2011;26:31–46.
10. Kaczor AA, Kronbach C, Unverferth K, Pihlaja K, Wiinamäki K, Sinkkonen J, Kijkowska-Murak U, Wróbel T, Stachal T, Matosiuk D. Novel non-competitive antagonists of kainate GluK1/GluK2 receptors. Lett Drug Des Discov. 2012;9:891–8.
11. Kaczor AA, Karczmarzyk Z, Fruziński A, Pihlaja K, Sinkkonen J, Wiinämaki K, Kronbach C, Unverferth K, Poso A, Matosiuk D. Structural studies, homology modeling and molecular docking of novel non-competitive antagonists of GluK1/GluK2 receptors. Bioorg Med Chem. 2014;22(2):787–95.
12. Valgeirsson J, Nielsen EØ, Peters D, Varming T, Mathiesen C, Kristensen AS, Madsen U. 2-Arylureidobenzoic acids: selective noncompetitive antagonists for the homomeric kainate receptor subtype GluR5. J Med Chem. 2003;46:5834–43.
13. Valgeirsson J, Nielsen EO, Peters D, Mathiesen C, Kristensen AS, Madsen U. Bioisosteric modifications of 2-arylureidobenzoic acids: selective noncompetitive antagonists for the homomeric kainate receptor subtype GluR5. J Med Chem. 2004;47:6948–57.
14. Kaczor AA, Wróbel T, Kronbach C, Unverferth K, Stachal T, Matosiuk D. Synthesis and molecular docking of novel non-competitive antagonists of GluK2 receptor. Med Chem Res. 2015;24:810–7.
15. Kaczor AA, Pihlaja K, Kronbach C, Unverferth K, Wrobel T, Stachal T, Matosiuk D. Synthesis and molecular docking of indole and carbazole derivatives with potential pharmacological activity. Heterocycl Commun. 2014;20:103–9.
16. Kaczor AA, Matosiuk D. Molecular structure of ionotropic glutamate receptors. Curr Med Chem. 2010;17:2608–35.
17. Stayte S, Vissel B. Advances in non-dopaminergic treatments for Parkinson's disease. Front Neurosci. 2014;8:113.
18. Crépel V, Mulle C. Physiopathology of kainate receptors in epilepsy. Curr Opin Pharmacol. 2015;20:83–8.
19. Szénási G, Vegh M, Szabo G, Kertesz S, Kapus G, Albert M, Greff Z, Ling I, Barkoczy J, Simig G, Spedding M, Harsing LG Jr. 2,3-Benzodiazepine-type AMPA receptor antagonists and their neuroprotective effects. Neurochem Int. 2008;52:166–83.
20. Kaczor AA, Kijkowska-Murak UA, Matosiuk D. Theoretical studies on the structure and symmetry of the transmembrane region of glutamatergic GluR5 receptor. J Med Chem. 2008;51(13):3765–76.
21. Kaczor AA, Kijkowska-Murak UA, Kronbach C, Unverferth K, Matosiuk D. Modeling of glutamate GluR6 receptor and its interactions with novel noncompetitive antagonists. J Chem Inf Model. 2009;49:1094–104.

22. Jamróz MH. On the internal coordinates in the Potential Energy Distribution (PED) analysis: bending or torsion? Enliven Bioinform. 2014;1:1–3.

23. Gaussian 09, Revision E.01, Frisch MJ, Trucks GW, Schlegel HB, Scuseria GE, Robb MA, Cheeseman JR, Scalman, G, Barone V, Mennucci B, Petersson GA, Nakatsuji H, Caricato M, Li X, Hratchian HP, Izmaylov AF, Bloino J, Zheng G, Sonnenberg JL, Hada M, Ehara M, Toyota K, Fukuda R, Hasegawa J, Ishida M, Nakajima T, Honda Y, Kitao O, Nakai H, Vreven T, Montgomery JA Jr, Peralta JE, Ogliaro F, Bearpark M, Heyd JJ, Brothers E, Kudin KN, Staroverov VN, Kobayashi R, Normand J, Raghavachari K, Rendell A, Burant JC, Iyengar SS, Tomasi J, Cossi M, Rega N, Millam JM, Klene M, Knox JE, Cross JB, Bakken V, Adamo C, Jaramillo J, Gomperts R, Stratmann RE, Yazyev O, Austin AJ, Cammi R, Pomelli C, Ochterski JW, Martin RL, Morokuma K, Zakrzewski VG, Voth GA, Salvador P, Dannenberg JJ, Dapprich S, Daniels AD, Farkas Ö, Foresman JB, Ortiz JV, Cioslowski J, Fox DJ. Wallingford: Gaussian Inc.; 2009.

24. Barnes L, Schindler B, Allouche AR, Simon D, Chambert S, Oomens J, Compagnon I. Anharmonic simulations of the vibrational spectrum of sulfated compounds: application to the glycosaminoglycan fragment glucosamine 6-sulfate. Phys Chem Chem Phys. 2015;17:25705–13.

25. Jamróz MH. Vibrational energy distribution analysis VEDA 4, Warsaw; 2004.

26. Jamróz MH. Vibrational energy distribution analysis (VEDA): scopes and limitations. Spectrochim Acta A. 2013;114:220–30.

27. Pitucha M, Sobotka-Polska K, Keller R, Pachuta-Stec A, Mendyk E, Kaczor AA. Synthesis and structure of new 1-cyanoacetyl-4-arylsemicarbazide derivatives with potential anticancer activity. J Mol Struct. 2016;1104:24–32.

28. Bartyzel A, Kaczor AA. The formation of a neutral manganese(III) complex containing a tetradentate Schiff base and a ketone–synthesis and characterization. J Coord Chem. 2015;68:3701–17.

29. Kaczor AA, Bartyzel A, Pitucha M, Wróbel TM, Woźniak S, Matosiuk D. Synthesis, experimental and computational studies of N-(4-amino-6-oxo-1,6-dihydropyrimidin-5-yl)benzamide. Lett Org Chem. 2018. https://doi.org/10.2174/1570178614666170811123851 (in press).

30. Bartyzel A, Kaczor AA. Synthesis, crystal structure, thermal, spectroscopic and theoretical studies of N_3O_2-donor Schiff base and its complex with Cu^{II} ions. Polyhedron. 2018;139:271–81.

31. Bartyzel A, Sztanke M, Sztanke K. Thermal studies of analgesic active 8-aryl-2,6,7,8-tetrahydroimidazo[2,1-c][1, 2, 4]triazine-3,4-diones. J Therm Anal Calorim. 2016;123:2053–60.

32. Bartyzel A, Sztanke M, Sztanke K. Thermal behaviour of antiproliferative active 3-(2-furanyl)-8-aryl-7,8-dihydroimidazo[2,1-c][1, 2, 4]triazin-4(6H)-ones. J Therm Anal Calorim. 2017;130:1541–51.

33. Bartyzel A. Effect of molar ratios of reagents and solvent on the complexation process of nickel(II) ions by the N_2O_3-donor Schiff base. Polyhedron. 2017;134:30–40.

34. Bartyzel A. Synthesis, thermal behaviour and some properties of Cu^{II} complexes with N,O-donor Schiff bases. J Therm Anal Calorim. 2018;131:1221–36.

35. Kanaoka Y, Ban Y, Oishi T, Yonemitsu O, Terashima M, Kimura T, Nakagawa M. Infrared spectra of some indole and pyrrole compounds. Chem Pharm Bull. 1960;8:294–301.

36. Sundaraganesan N, Umamaheswari H, Dominic Joshua B, Meganathan C, Ramalingam M. Molecular structure and vibrational spectra of indole and 5-aminoindole by density functional theory and ab initio Hartree–Fock calculations. J Mol Struc Theochem. 2008;850:84–93.

37. Saleem H, Subashchandrabose S, Erdogdu Y, Thanikachalam V, Jayabharathi J. FT-IR, FT-Raman spectral and conformational studies on (E)-2-(2-hydroxybenzylidenamino)-3-(1H-indol-3yl) propionic acid. Spectrochim Acta A. 2013;101:91–9.

38. Bunte SW, Jensen GM, McNesby KL, Goodin DB, Chabalowski CF, Nieminen RM, Suhai S, Jalkanen KJ. Theoretical determination of the vibrational absorption and Raman spectra of 3-methylindole and 3-methylindole radicals. Chem Phys. 2001;265:13–25.

39. Arjunan V, Puviarasan N, Mohanc S. Fourier transform infrared and Raman spectral investigations of 5-aminoindole. Spectrochim Acta A. 2006;64:233–9.

40. Morzyk-Ociepa B. Vibrational spectroscopic studies of indole-carboxylic acids and their metal complexes Part VIII. 5-Methoxyindole-2-carboxylic acid and its Zn(II) complex. Spectrochim Acta A. 2009;72:236–43.

41. Mello GS, Cardoso AP, Oliveira EWRS, Siqueira AB. Tryptophan a proposal of the mechanism of thermal decomposition. J Therm Anal Calorim. 2015;122:1395–401.